Journal of Alloys and Compounds 509 (2011) 6509–6517

Contents lists available at ScienceDirect

Journal of Alloys and Compounds

journal homepage: www.elsevier.com/locate/jallcom

Superstructure and magnetic properties of $R_{15}X_9C$ compounds (R = rare earth; X = Si and Ge)

F. Wrubl[a], K.V. Shah[b], Devang A. Joshi[b], P. Manfrinetti[a,c,*], M. Pani[a], C. Ritter[d], S.K. Dhar[b]

[a] Dipartimento di Chimica e Chimica Industriale, Universitá di Genova, Via Dodecaneso 31, 16146, Genova, Italy
[b] Department of Condensed Matter Physics & Material Science, T.I.F.R., Homi Bhabha Road, Mumbai 400005, India
[c] CNR-SPIN, Corso Perrone 24, 16152 Genova, Italy
[d] Institut Laue-Langevin, 6 Rue J. Horowitz, 38042 Grenoble, France

ARTICLE INFO

Article history:
Received 10 November 2010
Received in revised form 13 March 2011
Accepted 16 March 2011
Available online 22 March 2011

Keywords:
Rare-earth silicon carbide
Rare-earth germanium carbide
Crystal structure
Ferromagnetic ordering
Heat capacity
Kondo lattice

ABSTRACT

We report the synthesis of the new compounds $R_{15}Si_9C$ with R = Sm, Gd–Er, Y and $R_{15}Ge_9C$ with R = Ce, Pr and Nd. These compounds crystallize in the hexagonal $La_{15}Ge_9Fe$ structure type (hP50, $P6_3mc$, $Z = 2$) which is an ordered superstructure of La_5Ge_3 (Mn_5Si_3-type, hP16, $P6_3/mcm$, $Z = 2$). The superstructure is absent in a single-phase $R_5Ge_3C_{0.33}$ alloy with R = Sm and Gd. The addition of interstitial carbon modifies the magnetic properties significantly as regards the magnetic transition temperature and the nature of the magnetic ordering. Carbon doping induces mostly a ferromagnetic or ferrimagnetic configuration. The preponderance of ferromagnetic interactions in the superstructure compounds, with respect to the parent phases, can tentatively be attributed to a change in the sign of the RKKY interactions. The dense Kondo lattice state of Ce in ferrimagnetic Ce_5Ge_3 is preserved in $Ce_{15}Ge_9C$. Large coercive fields (~4–5 kOe) at low temperatures are observed in most compounds, which exceed ~50 kOe in the two Sm based compound.

1. Introduction

Most of the R_5X_3 intermetallics with R = rare earth and X = Ga, Si, Ge, Sn and Sb, crystallize in the hexagonal Mn_5Si_3-type structure (*hP*16–$P6_3/mcm$, space group No. 193) [1]. In this structure prototype the R atoms occupy the two inequivalent 4*d* and 6*g* crystal sites, i.e. the special positions (1/3, 2/3, 0) and (x_R, 0, ¼), respectively, while the X atoms occupy the 6*g* site (x_X, 0, ¼). The R atoms in 6*g* form chains of confacial trigonal antiprisms (octahedra), while the X atoms bridge all edges of the shared faces. A summary of the magnetic properties reported in literature for most of the R_5X_3 phases, with X = Si and Ge, is given into a next paragraph. A variety of elements can be alloyed interstitially in the centers of the antiprisms to produce stuffed versions of the same structure type. The alloying of carbon and of boron, for example, with some R_5X_3 compounds, resulted in the formation of interstitial compounds $Er_5Si_3C_x$, $Gd_5Si_3C_x$, $Ho_5Si_3C_x$, $Nd_5Ge_3B_x$ and $Dy_5Ge_3B_x$ for various values of x [2–4]. A new superstructure derived from the Mn_5Si_3-type La_5Ge_3 by the insertion of one interstitial atom Z per three Mn_5Si_3-type cells ($a' = \sqrt{3}a$, $c' = c$) has been found to exist in a series of La-compounds with the stoichiometry $La_{15}Ge_9Z$ (Z = C, Mn, Fe, Co, Ni, Cu, Ru, O and P) [5]. We report in the present work that the superstructure formation with C extends to $R_{15}Si_9C$ with R = Sm, Gd, Tb, Dy, Ho, Er and Y. In the case of Ge compounds the superstructure $R_{15}Ge_9C$ forms for R = Ce, Pr and Nd, but not for R = Sm and Gd; for these two rare earths only formation of $R_5X_3C_{0.33}$ stuffed phases has been observed. Preliminary results on the existence and on the magnetic behavior of the two families have already been anticipated [6]; here we report on their magnetic and some physical properties, too. Significant modifications of the magnetic properties of the parent R_5Si_3 and R_5Ge_3 take place with the addition of interstitial carbon.

2. Experimental details

The samples were prepared by arc melting, in an inert atmosphere of argon, weighed amounts of rare earths (99.9 wt.% purity), germanium or silicon (99.999 wt.% purity) and carbon (6 mm-diameter rod, spectroscopic grade). A typical procedure consisted in melting the R metal with C first, forming the corresponding carbide, and then melting together the preformed carbide with germanium or silicon. The samples were turned upside-down and re-melted at least three times in order to ensure complete carbon dissolution and homogenization. An alternative method of reacting carbon with preformed R_5Ge_3 proved to be unsuccessful as it resulted in both carbon and total weight losses. The as-cast alloys, placed inside open out-gassed Ta crucibles and sealed under vacuum into quartz ampoules, were annealed at 1000 °C for 14–21 days, followed by a fast air-cooling. The compounds were characterized by X-ray powder diffraction, using a Guinier camera, with pure Si as internal standard ($a = 5.4308$ Å) and Cu $K\alpha_1$ radiation. Rietveld refinements were performed on all the phases to confirm the single-phase state, by means of the FullProf program [7] on patterns collected on a Bragg–Brentano Panalytical instrument,

* Corresponding author. Tel.: +39 010 3536081; fax: +39 010 3628252.
E-mail address: chimfis@chimica.unige.it (P. Manfrinetti).

0925-8388/$ – see front matter © 2011 Elsevier B.V. All rights reserved.
doi:10.1016/j.jallcom.2011.03.092

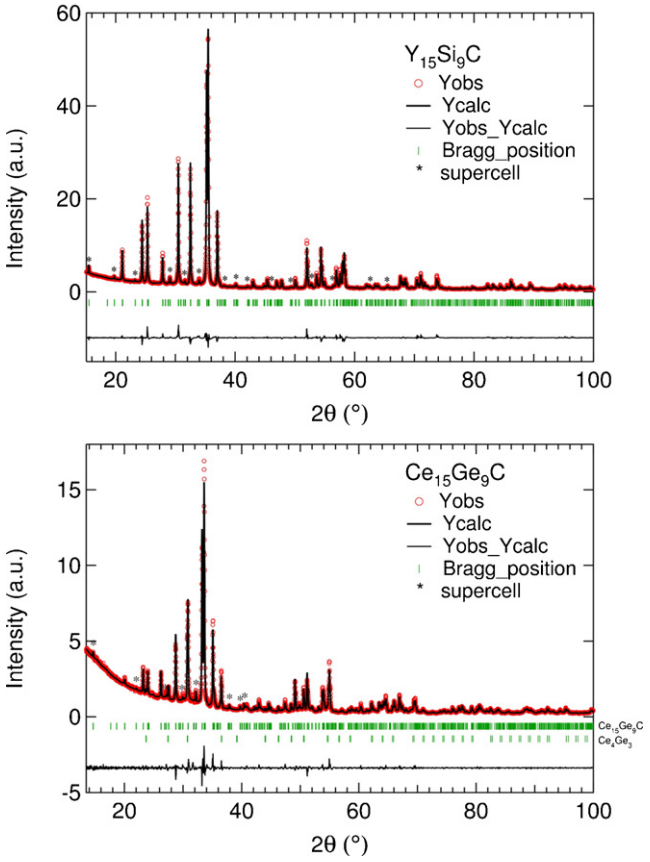

Fig. 1. The X-ray powder patterns of $Y_{15}Si_9C$ and $Ce_{15}Ge_9C$, taken as representative examples of the 15:9:1 silicides and germanides, respectively.

with Cu Kα radiation. Single crystals were mounted on a Bruker-Nonius MACH3 diffractometer with graphite monochromated Mo Kα radiation (see supplementary material for details of data collection conditions). The computer programs SHELXS-97 [8] and SHELXL-97 [9] were employed for single crystal structure solutions and refinements. Crystal calculations were performed with the Bond_Str program, part of the Fullprof suite. Structure drawings were made with the DrawXtl program [10]. Micrographic analysis by optical and electron microscopy (SEM) was also performed on portions of the samples. Magnetization was measured using SQUID and VSM magnetometers while resistivity, magnetoresistivity and heat capacity were recorded on PPMS (Quantum Design).

3. Results and discussion

3.1. Crystallographic properties

The alloys were all single, or nearly single, phase. La, Ce and Pr samples of $R_{15}Ge_9C$ contained only a few % of extra phases, mainly the binary compound R_4Ge_3 (anti-Th_3P_4 type); no trace of secondary phases were found for R = Nd, Sm and Gd among the germanides and for all the $R_{15}Si_9C$ compounds. Indexing of the reflections in the powder patterns was carried out by comparing the observed intensities with those calculated by the Lazy-Pulverix program [11] on the basis of the atomic positions reported for the known $La_{15}Ge_9Fe$-type single crystal data [5]. Fig. 1 shows the Bragg–Brentano X-ray diffractograms of $Y_{15}Si_9C$ and $Ce_{15}Ge_9C$ phases. In both patterns the low-intensity superstructure reflections, absent in the parent binary phase, are unambiguously visible (highlighted with an asterisk). The Guinier pattern of the Sm and Gd stuffed germanides, when compared with the parent compounds [2] were only slightly shifted to the left (due to a volume expansion of 1.2% and of 0.2% respectively), and no superstructure reflections were detectable. Therefore we here refer to them as $Sm_5Ge_3C_{0.33}$ and $Gd_5Ge_3C_{0.33}$. However, as reported in the magnetic properties section, it should be noted that the stuffed Sm germanide, if compared to the parent compound, behaves in a significantly different way and orders ferromagnetically, as the $R_{15}Ge_9C$ phases do, while the behavior of the Gd germanide is strictly related to that of the host compound.

Presumably, the heavier rare earths (from Tb onwards) form as well the partially stuffed $R_5Ge_3C_{0.33}$ (or $R_5Ge_3C_x$). The radii ratio r_R/r_X is found to be ≥1.33 in all the $R_{15}X_9C$ compounds and the geometric factor might be related to the superstructure formation, in analogy with the formation of the Mn_5Si_3-type R_5X_3 compounds. In fact the two structures are strictly related and formed by layers containing both metals and non-metals [2]. The elements La to Nd do not form partially stuffed silicides because they form different binary Cr_5B_3-type parent phases, rather than Mn_5Si_3-type (only Nd has been reported to shift to the Mn_5Si_3 structure type in the fully stuffed Nd_5Si_3C compound [2]). The lattice parameters of $R_{15}X_9C$, listed in Table 1, follow a decreasing linear trend, like expected from the lanthanide contraction. The formation volume–contraction ΔV_f is slightly higher for the silicides (11% av.) than for the germanides (7.2% av.). The appearance of the superstructure, due to the ordered carbon insertion in the 5:3 frame, implies a small volume expansion (ΔV_p, 1.1% av.) of the starting host phases.

The $La_{15}Ge_9C$ structure type was confirmed from the results of the single crystal analysis for $Nd_{15}Ge_9C$: in this compound, the carbon position was unambiguously localized (see atomic coordinates in Table 2) from the difference Fourier map, after anisotropic refinement of Nd and Ge atoms. The complete structural model converged to acceptable agreement indexes (wR2 = 0.073, R1 = 0.036), and at the end of the refinement procedure, the peaks of residual electron density were found in correspondence of neodymium atoms only [1].

The result obtained for the Nd compound was thus extended to all other 15:9:1 phases and Rietveld refinements were performed using the $La_{15}Ge_9Fe$ atomic positions as starting point. R and X positions were refined first, while carbon was included only in the last stage, fixed in the calculated cavity center around (1/3 2/3 ~0.5). A global thermal parameter was refined for the Sm and Er silicides; in all other compounds, isotropic displacement parameters could be refined as independent values for groups of atomic species. Due to the low atomic number of carbon, X-ray powder data did not allow to exclude that C is also partly accommodated into other available cavities [2].

The 5:3 structure and the 15:9:1 superstructure are strictly related, the volume of the 15:9:1 supercell being three times larger than that of the 5:3 parent cell. The relationship between the two unit cells is depicted in the [0 0 1] projection of Fig. 2. The supercell arises as a result of regular small atomic shifts in the parent structure that accompany the ordered insertion of interstitial atoms. While the R atoms occupy the two in-equivalent 4*d* and 6*g* sites in R_5X_3 unit cell (*hP*16, $P6_3/mcm$), four symmetry in-equivalent rare-earth sites are needed to describe the $R_{15}X_9C$ unit cell (one 12*d* and three 6*c* Wyckoff positions, *hP*50, $P6_3mc$), as drawn in Fig. 2. The Mn_5Si_3-type unit cell possesses 2 octahedral rare-earth cavities, i.e.: one cavity per unit formula, in which small atomic species can be accommodated. While in the stuffed $R_5X_3C_x$ compounds the C atoms randomly occupy both the available 2*b* octahedral cavities formed by the 6*g* R atoms, up to the maximum extent ($x = 1$) [2], in the triple cell of the stoichiometric $R_{15}X_9C$, only one third of all the

[1] Single crystal intensity data were also collected for $Dy_{15}Si_9C$ and $Er_{15}Si_9C$: in these compounds, however, probably due to absorption problems combined with the low diffraction power of carbon, some doubts still remain whether the C atoms only fill the 2*b* cavity at (1/3 2/3 ~0.5), or if they also partially enter the two other available cavities (2*b* at 1/3 2/3 ~0; 2*a* at 0 0 ~0).

[2] Atomic coordinates are deposited as supplemental data file.

Table 1
Lattice parameter values, a and c (as obtained by Guinier powder patterns), unit cell volume V_U, and the resulting formation volume–contraction, ΔV_f, for the $R_{15}Si_9C$ (R = Sm, Gd, Tb, Dy, Ho, Er, Y) and $R_{15}Ge_9C$ (R = La, Ce, Pr, Nd) compounds ($La_{15}Ge_9Fe$-type, $hP50$, $P6_3mc$, $Z = 2$). ΔVp is the volume expansion due to the C addition, with respect to the parent phase.

Compound	a (Å)	c (Å)	V_U (Å^3)	ΔV_f (%)	ΔV_p (%)
$Sm_{15}Si_9C$	14.845(1)	6.561(1)	1252.2(4)	8.8	1.03
$Gd_{15}Si_9C$	14.725(2)	6.435(2)	1208.3(7)	11.9	0.27
$Tb_{15}Si_9C$	14.629(1)	6.418(1)	1189.5(3)	11.4	2.26
$Dy_{15}Si_9C$	14.537(1)	6.348(1)	1161.7(3)	12.2	1.15
$Ho_{15}Si_9C$	14.459(1)	6.325(1)	1145.1(3)	12.7	1.39
$Er_{15}Si_9C$	14.410(2)	6.285(1)	1130.2(5)	12.9	1.77
$Y_{15}Si_9C$	14.573(1)	6.404(1)	1177.8(3)	14.2	1.18
$La_{15}Ge_9C$[a]	15.467(1)	6.880(1)	1425.4(4)	7.9	−0.74
$Ce_{15}Ge_9C$	15.336(2)	6.791(1)	1383.2(6)	5.8	1.38
$Pr_{15}Ge_9C$	15.242(2)	6.764(2)	1360.8(8)	6.9	1.79
$Nd_{15}Ge_9C$	15.129(2)	6.713(1)	1330.6(6)	8.3	1.59
$Sm_5Ge_3C_{0.33}$	8.655(1)	6.574(1)	426.5(2)	8.8	1.17
$Gd_5Ge_3C_{0.33}$	8.5547(7)	6.4681(7)	409.9(1)	12.2	0.23

[a] Data from reference [5].

six available cavities per unit cell is occupied, as indicated by the stoichiometric formula, but the insertion takes place in an ordered fashion. The overall six cavities in the enlarged unit cell are formed by R2(6*c*)–R3(6*c*) and R4(6*c*)–R4(6*c*) atoms, but the two occupied, as in the $La_{15}Ge_9Fe$ prototype, are those formed by the R2 and R3 atoms only, as depicted in the lower part of Fig. 2 (projection along the [1 1 0] direction).

The shortest R–R distances (12*d*–12*d*) are reported in Table 3 for each 15:9:1 compound, alongside with the shortest R–R distance (4*d*–4*d*) in the parent 5:3 phase. In both structures these atoms form long chains along the *c* axis, and the interaction has a covalent character, as suggested by the radii of the 12*d* rare-earth atoms, comparable with their covalent values. The structure change induced by the ordered insertion of carbon causes an increase in these R–R distances (2% av. for 12*d*–12*d*, $\Delta d = 0.04$–0.09 Å). Table 3 also reports the octahedral cavity radii r_{Cav}, calculated as $r_{Cav} = d_{R-C} - r_R$ where d_{R-C} is the R–C distance at the cavity center and r_R is the rare earth atomic radius (CN12, [12]). The cavity radii range from 0.84 Å (for $Ce_{15}Ge_9C$) to 0.66 Å (for $Dy_{15}Si_9C$). They clearly follow the rare-earth dimensions trend and are distributed around the value of 0.77 Å (carbon covalent radius, smaller than the corresponding CN12 atomic radius of 0.91 Å [12]). In ref. [5] it has clearly been underlined that in the $La_{15}Ge_9Z$ family of compounds the La2–La3 antiprisms give rise to a 'Peierls-like' distortion, being alternately longer and shorter if empty or filled. In agreement with this remark, in all the $R_{15}X_9C$ phases, the filled R2–R3 cavities turn out to be considerably compressed if compared to the corresponding R_5X_3C filled antiprisms. The 15:9:1 cavity radii are shown in Table 3, in comparison with those of the 5:3:1 values; on average, they are smaller by 14%: the silicide cavities are smaller by 16.5% av. (with peak contractions of 20% for Gd and Dy), while the germanide ones get smaller by 8% av., the dimensions in the Ce compound being thereby the less affected by the superstructure formation (−4%). The reduction of the cavity dimension in the $R_{15}X_9C$ compounds suggests an increase of the covalent character of the six R–C bonds (either R2–C or R3–C); this reminds, in analogy with what has been concluded for other rare-earth carbides (like GdC_x, $x \sim 0.33$, [13]), that the increased overlap that occurs between 2p–C and 4*f*–R orbitals, determines an increase in the interaction between the cavity-forming R2–R3 atoms. This factor, together with the symmetry change in passing from the 5:3 to the 15:9:1 structure, likely contributes to the ultimate dramatic change of the magnetic properties discussed in the following paragraph.

3.2. Magnetic properties

3.2.1. Summary of magnetism of the R_5X_3 phases

We first briefly summarize the magnetic behavior of the parent R_5Ge_3 and R_5Si_3 compounds, in order to compare the changes induced by the interstitial addition of carbon. Despite their simple formula these compounds present rather complicated magnetic structures, associated with one or both the R sublattices. The magnetic properties of R_5Ge_3 compounds were first reported by Buschow and Fast [14]; antiferromagnetic ordering at 12 and 48 K was seen in Pr_5Ge_3 and Gd_5Ge_3 respectively, while Nd_5Ge_3 was inferred to be ferrimagnetic below 45 K. Subsequently, while the type of magnetic ordering was confirmed for Gd_5Ge_3 (but with a $T_N = 80$ K [15]), a neutron diffraction study on Nd_5Ge_3 showed that it orders antiferromagnetically at 52 K, with a collinear double-sheet structure for the Nd ions at the 6*g* site and a canted structure for the ions at the 4*d* site [16]. Studies on Ce_5Ge_3 have revealed that it is a dense Kondo lattice exhibiting a complex magnetic structure with spontaneous magnetization below 6.4 K [17]. Magnetization data on a single crystal of Gd_5Ge_3 have shown a cusp at 76 K followed by a shoulder at 52 K, indicating two antiferromagnetic transitions [18]. Conical magnetic ordering in Tb_5Si_3 [19], Dy_5Si_3 [20], collinear for Er_5Si_3 [21], flat spiral for Tb_5Ge_3 [22] have been reported. More recently, a complex sine-modulated type of magnetic ordering has been shown for Ho_5Si_3 and Ho_5Ge_3, both presenting on cooling two subsequent antiferromagnetic orderings [23], while a sine-

Table 2
Fractional atomic coordinates and anisotropic displacement parameters for $Nd_{15}Ge_9C$, $La_{15}Ge_9C$ type, hexagonal, $hP50$–$P6_3mc$, $Z = 2$, as obtained from single crystal X-ray analysis. Agreement indexes: wR2 = 0.073, R1 = 0.036, Goodness of fit GoF = 0.842.

Atom	Wyckoff site	x	y	z	U_{eq} [Å^2]
Nd1	12*d*	.01681(6)	.34169(8)	0	.0114(2)
Nd2	6*c*	.41259(8)	2*x*	.7355(7)	.0112(4)
Nd3	6*c*	.25436(8)	2*x*	.2830(7)	.0077(4)
Nd4	6*c*	.07930(8)	2*x*	.7360(8)	.0147(4)
Ge1	6*c*	.1331(2)	2*x*	.273(1)	.0127(10)
Ge2	6*c*	.4669(2)	2*x*	.262(1)	.0113(8)
Ge3	6*c*	.1991(2)	2*x*	.717(1)	.0100(9)
C	2*b*	1/3	2/3	.512(9)	.007(5)

Table 3
Shortest R–R interatomic distances [Å] in the $R_{15}X_9C$ (12*d*–12*d*) and in the parent R_5X_3 compounds (4*d*–4*d*), cavity radii [Å] and Rietveld refinement agreement indexes, R_B, R_F, R_{wp} and R_p [%].

Compound	$R_{15}X_9C$ R–R	R_5X_3 R–R [a]	$r_{Cav.\ 15:9:1}$	$r_{Cav.\ 5:3:1}$ [a]	R_B	R_F	R_{wp}	R_p
$Sm_{15}Si_9C$	3.308(3)	3.24(1)	0.736(10)	0.845(10)	6.41	5.01	5.74	4.14
$Gd_{15}Si_9C$	3.244(1)	3.19(1)	0.671(5)	0.835(10)	2.30	1.85	3.47	2.62
$Tb_{15}Si_9C$	3.2283(6)	3.15(1)	0.699(10)	0.815(10)	6.26	5.24	5.25	3.52
$Dy_{15}Si_9C$	3.1899(5)	3.14(1)	0.661(7)	0.825(10)	4.09	2.48	3.69	2.72
$Ho_{15}Si_9C$	3.1796(6)	3.12(1)	0.684(6)	0.820(10)	6.04	3.90	5.78	4.17
$Er_{15}Si_9C$	3.1493(6)	3.11(1)	0.707(6)	0.815(10)	4.60	2.78	6.02	4.27
$Y_{15}Si_9C$	3.2145(5)	3.16(1)	0.677(5)	0.830(10)	4.76	4.53	5.44	4.05
$Ce_{15}Ge_9C$	3.4224(7)	3.36(1)	0.839(6)	0.870(10)	5.33	3.24	5.59	3.94
$Pr_{15}Ge_9C$	3.413(1)	3.33(1)	0.798(8)	0.870(10)	8.00	5.40	7.94	4.63
$Nd_{15}Ge_9C$	3.3883(7)	3.30(1)	0.764(12)	0.865(10)	4.04	2.79	7.63	4.79

[a] Data from reference [2].

modulated collinear antiferromagnetic structure has been found in Er_5Ge_3 [24]. It may be noted that overall the magnetic interactions in both R_5Si_3 and R_5Ge_3 compounds are antiferromagnetic. The crystal electric fields at the two in-equivalent rare earth sites are different giving rise to anisotropy directions which are perpendicular to each other in some of these compounds.

3.2.2. *Magnetic properties of the $R_{15}X_9C$ compounds*

At 300 K, all the $R_{15}X_9C$ compounds studied in the present work are paramagnetic. At high temperatures, the inverse susceptibility of nearly all the compounds shows a Curie Weiss behavior, except $Pr_{15}Ge_9C$, $Sm_{15}Si_9C$ and $Sm_5Ge_3C_{0.33}$. Some representative

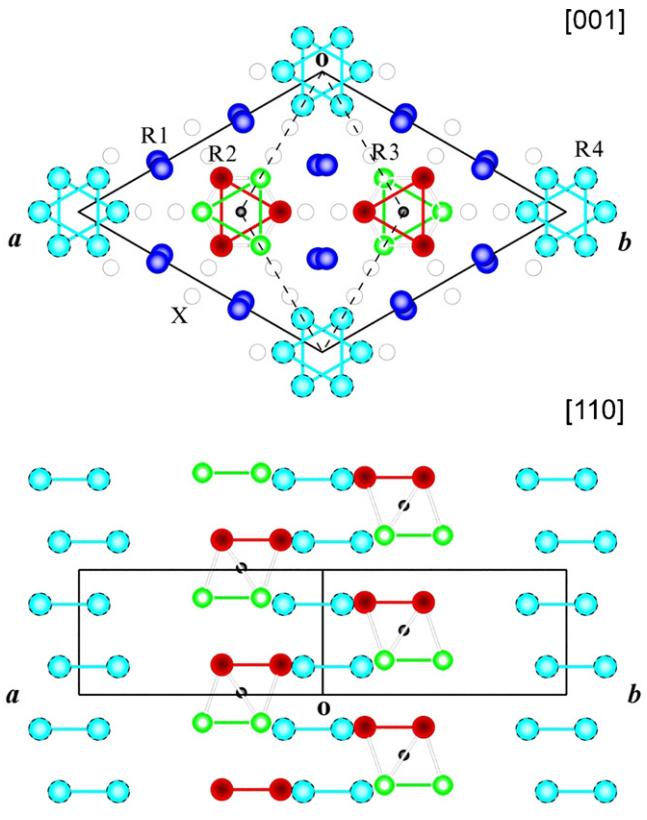

Fig. 2. (Color online) The $R_{15}X_9C$ unit cell viewed along [0 0 1]. Atoms R1 (12*d*, blue), R2 (6*c*, red), R3 (6*c*, green), R4 (6*c*, cyan), X (6*c*, white), C (2*b*, black) are shown. The parent R_5X_3 (Mn_5Si_3-type) unit cell is shown as dashed line. R atoms forming trigonal antiprims are connected intra-plane (same color as atoms); R forming occupied cavities are connected also inter-plane (white lines), to highlight the filled octahedra. The $R_{15}X_9C$ unit cell viewed along [1 1 0]. R1 and X atoms are hidden for clarity purpose. (For interpretation of the references to color in the text, the reader is referred to the web version of the article.)

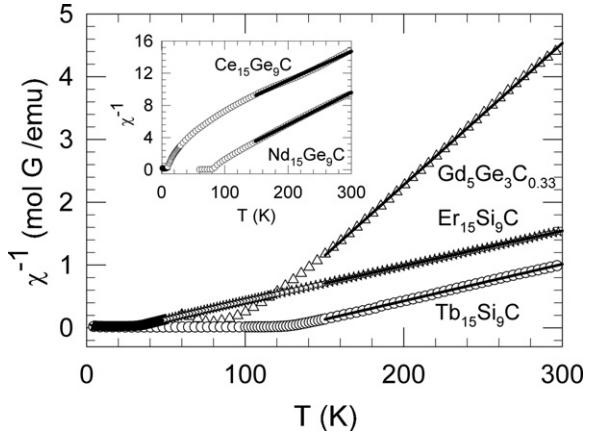

Fig. 3. The Curie–Weiss variation of the inverse susceptibility, χ^{-1}, of $Er_{15}Si_9C$, $Tb_{15}Si_9C$ and $Gd_5Ge_3C_{0.33}$. The inset shows the data for $Ce_{15}Ge_9C$ and $Nd_{15}Ge_9C$.

plots are shown in Fig. 3. The paramagnetic Curie temperatures, θ_p, obtained by fitting the Curie–Weiss expression $\chi = C_{cw}/(T - \theta_p)$ to the susceptibility data are positive, except in $Ce_{15}Ge_9C$, indicating *prima facie* a ferromagnetic exchange interaction between the rare earth ions. The effective paramagnetic moments are close to the free ion values (see Table 4), slight deviations being attributed to conduction electron polarization and or stoichiometry of the sample, save for $Ce_{15}Ge_9C$, where it is appreciably larger. The negative θ_p in $Ce_{15}Ge_9C$ may arise from a single ion Kondo exchange interaction as discussed later. The magnetic susceptibility of $La_{15}Ge_9C$ and $Y_{15}Si_9C$ was measured between 1.8 and 300 K and they show typical Pauli paramagnetic behavior with $\chi_{4.2\,K} \sim 10^{-4}$ emu/g atom.

3.2.2.1. $R_{15}Si_9C$ compounds. The magnetization behavior of $R_{15}Si_9C$ (R = Sm, Gd, Tb, Dy, Ho and Er), which form in the ordered ternary structure, is consistent with a ferromagnetic ground state in the silicides. The hysteresis loops for R = Tb, Dy and Ho at 4.5 K, for example, are shown in Fig. 4. The initial rapid build-up of the magnetization followed by saturation at higher fields, the observation

Table 4
The effective paramagnetic moment per rare earth ion, μ_{eff}/R-ion, paramagnetic Curie temperature θ_p of $R_{15}Si_9C$ and $R_{15}Ge_9C$ compounds.

Compound	μ_{eff}/R-ion [μ_B]	θ_p [K]
$Gd_{15}Si_9C$	8.4	168.6
$Tb_{15}Si_9C$	9.5	127.0
$Dy_{15}Si_9C$	11.0	69.9
$Ho_{15}Si_9C$	10.7	36.6
$Er_{15}Si_9C$	9.8	23.2
$Ce_{15}Ge_9C$	3.84	−108.2
$Nd_{15}Ge_9C$	3.65	59.8
$Gd_5Ge_3C_{0.33}$	8.4	99.2

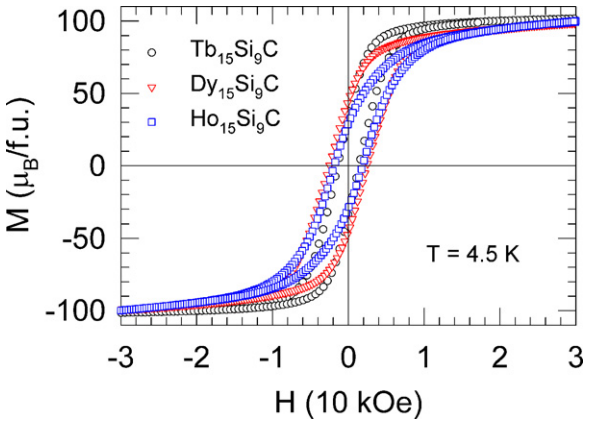

Fig. 4. The hysteresis loops of $R_{15}Si_9C$ (R = Tb, Dy and Ho) at 4.5 K.

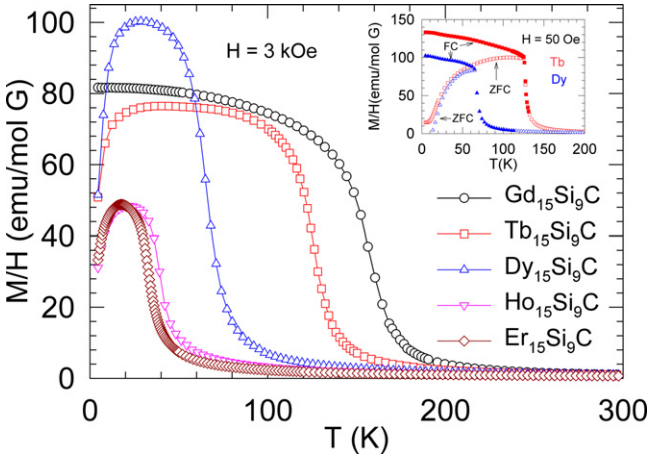

Fig. 5. The magnetization, M/H, (H = 3 kOe) below 300 K of $R_{15}Si_9C$ (R = Gd, Tb, Dy, Ho and Er). The inset shows the ZFC and FC magnetization M/H (H = 50 Oe) below 200 K for Tb and Dy compounds.

of a remanent magnetization and coercivity are characteristic signatures of the ferromagnetic ground state in these compounds. The saturation magnetization is less than the free ion value due to the effect of crystal electric fields. The coercive fields at 4.5 K are 1.5, 2.5 and 1.8 kOe for Tb, Dy and Ho compounds, respectively. The low field (50–100 Oe) ZFC and FC plots of magnetization are shown in the inset of Fig. 5 and in Fig. 6. The Curie temperature (inferred approximately from the sharp upturn of magnetization)

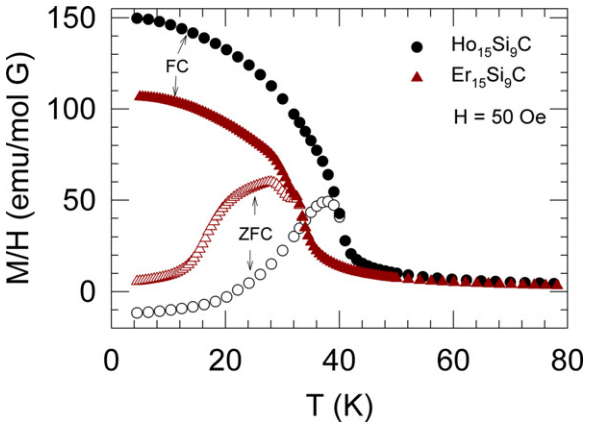

Fig. 6. The low field ZFC and FC magnetization, M/H, (H = 50 Oe) of $Ho_{15}Si_9C$ and $Er_{15}Si_9C$.

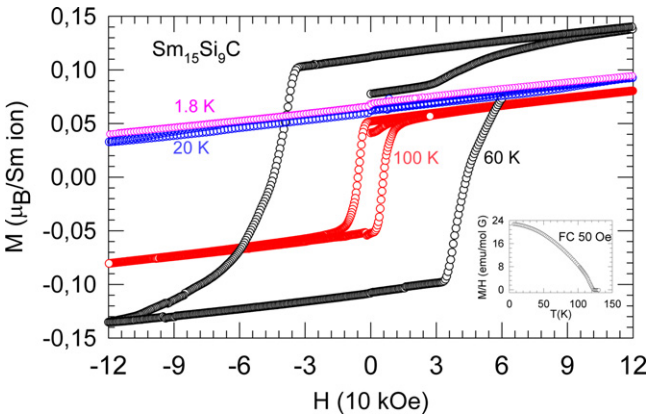

Fig. 7. The hysteresis loops of $Sm_{15}Si_9C$ at 1.8, 20, 60 and 100 K. The inset shows the FC magnetization, M/H, below 150 K in a field of 50 Oe.

is the highest in $Gd_{15}Si_9C$ and decreases with the increase in the atomic number of the rare earth (Fig. 5), which is qualitatively in accordance with the de Gennes scaling behavior. The deviation of the ZFC and FC plots from each other below T_C arises due to the large coercivity of these compounds. The shape of the magnetization plots in applied field of 3 kOe (Fig. 5), when the samples were cooled in zero field, most-likely arises due to an inter-play of the temperature variation of coercivity and magnetization below T_C. It appears unlikely to be due to the influence of any antiferromagnetic correlations as the low-field FC plots do not show any signature of antiferromagnetic transition.

$Sm_{15}Si_9C$ orders ferromagnetically at a temperature of ~120 K (see inset of Fig. 7). The coercive field at 60 K is nearly 45 kOe, taken as the average of the field values at which the magnetization crosses the M = 0 axis on up and down field cycles, which is large and higher than the corresponding value for the germanide at the same temperature. The magnetization at all fields at 20 and 1.8 K is lower than the corresponding values at 60 K and shows a behavior similar to that of a paramagnet or an antiferromagnet.

3.2.2.2. $R_{15}Ge_9C$ compounds. The low-field magnetization of $Ce_{15}Ge_9C$ in the zero-field-cooled (ZFC) and field-cooled (FC) modes is shown in Fig. 8. The upturn in the magnetization near 10 K and its subsequent variation with temperature, as the sample is cooled to 2 K in applied field of 50 Oe, suggests a ferromagnetic alignment of the moments in the field. The ZFC data, however, cross the M = 0 axis near 7.4 K, taking negative values at lower tem-

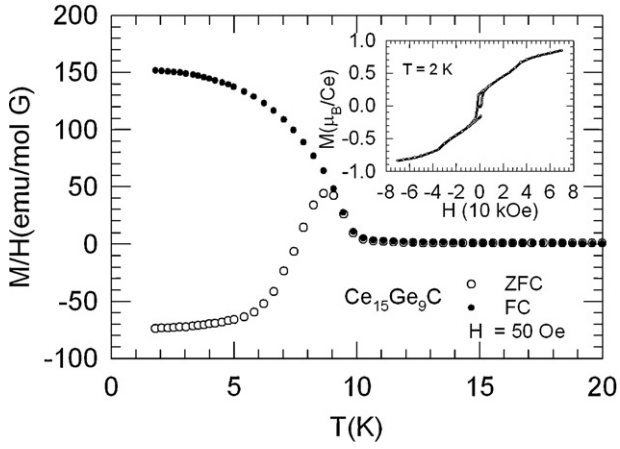

Fig. 8. The magnetization, M/H (H = 50 Oe) of $Ce_{15}Ge_9C$ below 20 K in ZFC and FC modes. The inset shows the hysteresis plot at 2 K up to a maximum applied field of 70 kOe.

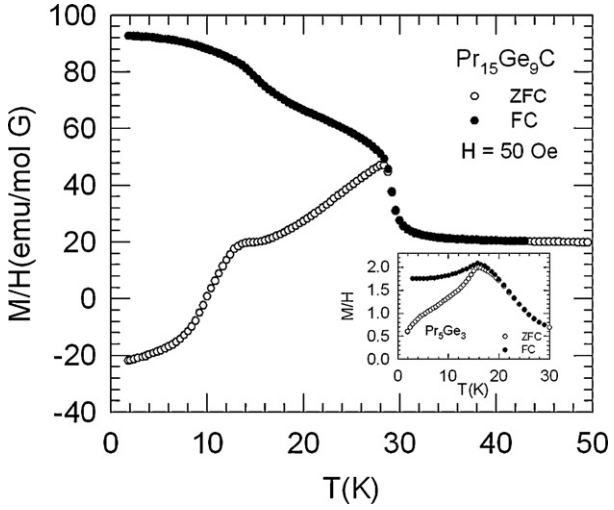

Fig. 9. The magnetization, M/H (H = 50 Oe) of $Pr_{15}Ge_9C$ below 50 K in ZFC and FC modes. The corresponding data for Pr_5Ge_3 below 30 K is shown in the inset.

peratures. Such a behavior suggests that the Ce moments adopt a ferrimagnetic like configuration when cooled in nominal zero field. An antiferromagnetic or a ferrimagnetic ground state which develops a spontaneous magnetization below 6.4 K has been postulated in the parent Ce_5Ge_3 [17]. The hysteresis loop of Ce_5Ge_3 at 2 K shows a coercive field of 1.2 kOe and the magnetization attains a value of 0.9 μ_B/Ce ion at 145 kOe without showing any signs of saturation. The coercive field of $Ce_{15}Ge_9C$ at 2 K is comparable with a magnitude of 2 kOe and the hysteresis loop indicates an additional contribution besides the ferromagnetic-like component which is responsible for the rapid initial rise of the magnetization with field. This may either arise due to the complex nature of the magnetic ordering involving Ce ions at four in-equivalent symmetry sites or alternatively some Ce ions may be in a Kondo/mixed valence state depending upon the degree of hybridization of the respective 4*f* orbital with the conduction electrons. In Ce_5Ge_3 a negative θ_p of 30.9 K was obtained from the magnetization data and the magnetic part of the resistivity, ρ_{4f}, showed two regions of $-\ln T$ dependence characteristic of a Kondo lattice compound [17]. We believe that a negative value of θ_p in $Ce_{15}Ge_9C$, which in absolute magnitude is far larger than that of Ce_5Ge_3, has a contribution derived from the Kondo interaction of some Ce ions in the lattice. It is likely that the magnetic state of some Ce ions is nearly non-magnetic due to their hybridization with the conduction electrons. The thermal variation of the magnetic susceptibility of such Ce ions will not follow the Curie–Weiss behavior characteristic of local moments. This might account for a not very good linear behavior of χ^{-1} versus T at high temperatures in $Ce_{15}Ge_9C$ (see the inset of Fig. 3) and also for an effective paramagnetic moment larger than the free ion value combined with a large negative θ_p of 108.2 K.

Fig. 9 shows the variation of both the ZFC and FC, low-field (50 Oe) magnetization in $Pr_{15}Ge_9C$ and, for the sake of comparison, in Pr_5Ge_3 (inset, Fig. 9). The Curie temperature, T_C, of $Pr_{15}Ge_9C$ is close to 30 K as inferred from the thermal variation of the low-field magnetization. The ZFC magnetization attains negative values below 10 K indicating a ferrimagnetic configuration similar to the case of $Ce_{15}Ge_9C$. The magnetic response of Pr_5Ge_3 is different. The peak near 16 K in Pr_5Ge_3 is a signature of the antiferromagnetic ordering of Pr ions in agreement with the previous results [12], though a minor divergence between the ZFC and FC data in the ordered state suggests a complex nature of antiferromagnetic configuration which is almost generic to R_5X_3 (X = Ge, Si, Sn and Sb) compounds, as mentioned above. Indeed, our recent single crystal magnetization data on Pr_5Ge_3 reveals an antiferromagnetic

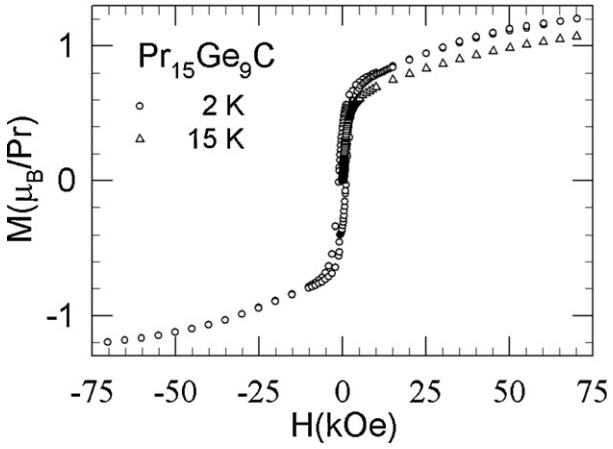

Fig. 10. The field dependence of magnetization of $Pr_{15}Ge_9C$ at 2 and 15 K up to 70 kOe.

transition at 13 K and a ferromagnetic-like upturn at 36 K when the applied field is parallel to *ab*-plane. A single ferrimagnetic-like transition at 13 K occurs when the field is applied along the *c*-axis [25]. The in-field magnetization plots of $Pr_{15}Ge_9C$ at 15 and 2 K are shown in Fig. 10. The sharp increase in the magnetization of $Pr_{15}Ge_9C$ at relatively low fields is in conformity with a ferromagnetic transition near 30 K. However, the magnetization both at 15 and 2 K (1.2 μ_B/Pr), does not saturate up to the highest applied field of 70 kOe. Similar to the case of Ce ions in $Ce_{15}Ge_9C$, the site-dependent magnetic response of four symmetry in-equivalent Pr ions, together with the evidence for a ferrimagnetic-like transition at lower temperature (Fig. 9), gives rise to the observed behavior of magnetization in the Pr compound.

Fig. 11 (lower inset) shows the ac susceptibility χ_{ac} of $Nd_{15}Ge_9C$ and the parent Nd_5Ge_3. The two peaks in χ_{ac} of Nd_5Ge_3 are in apparent conformity with the results of ref. [14]. However, in the carbide there is only one magnetic transition which occurs at T_C = 80 K. The ferromagnetic nature of the transition is inferred from the low field (100 Oe) ZFC and FC magnetization data below 100 K (upper inset) and from the hysteresis plot at 5 K. A large coercive field (~5 kOe at 5 K) is responsible for thermomagnetic irreversibility observed in low-field (100 Oe) magnetization of $Nd_{15}Ge_9C$. The saturation magnetization of 1.6 μ_B/Nd at 5 K, which is less than the free ion value, reflects the effect of crystal electric fields.

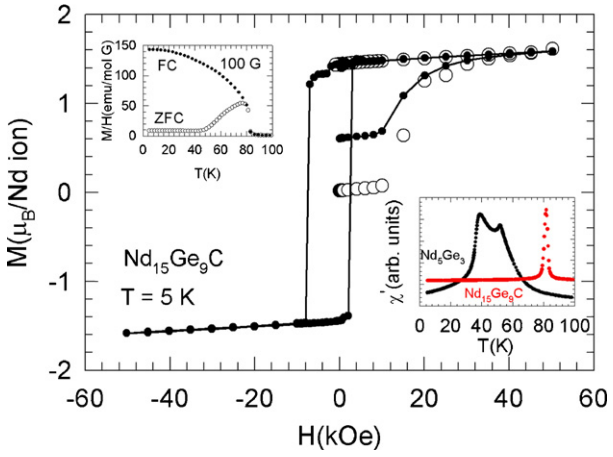

Fig. 11. The hysteresis loop of $Nd_{15}Ge_9C$ at 5 K. The upper inset shows the magnetization M/H (H = 100 Oe) in ZFC and FC modes below 100 K. The lower inset shows the ac susceptibility of Nd_5Ge_3 and $Nd_{15}Ge_9C$ below 100 K.

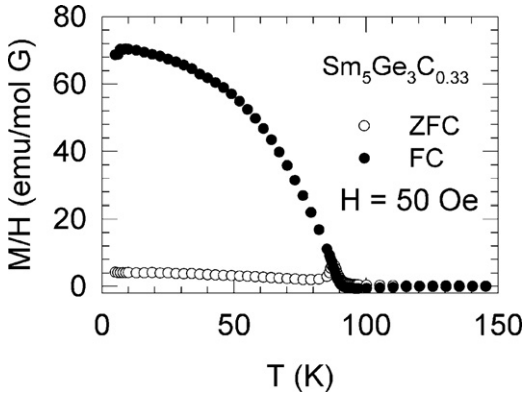

Fig. 12. The magnetization, M/H ($H = 50$ Oe) of $Sm_5Ge_3C_{0.33}$ in ZFC and FC modes below 150 K.

The FC and ZFC (50 Oe) magnetization data (Fig. 12) provide evidence for a ferromagnetic transition in $Sm_5Ge_3C_{0.33}$ as well, at $T_C \sim 88$ K, which is even higher than that in the Nd analog (but lower than that of $Sm_{15}Si_9C$). The isothermal magnetization at selected temperatures of 60, 40, 20 and 1.8 K is shown in Fig. 13. A large coercive field of nearly ~34 kOe, taken as the average of the field values at which the magnetization crosses the $M = 0$ axis on up and down field cycles, is observed at 60 K. The coercive field increases to 80 kOe as the temperature is lowered at 40 K. At 1.8 K the variation of the magnetization with field is surprisingly nearly linear and mimics that of a paramagnet or an antiferromagnet. The apparent lack of hysteresis at low temperatures in both $Sm_{15}Si_9C$ and $Sm_5Ge_3C_{0.33}$ is surprising and it needs further study to understand the observed behavior; it may arise due to the very high values of the coercive field at low temperatures, such that the applied field is not sufficient to induce significant rearrangement of domains in these two compounds.

While both the transition temperatures and the nature of magnetic ordering change markedly in the Pr and Nd analogs and in $Sm_5Ge_3C_{0.33}$, $Gd_5Ge_3C_{0.33}$ (in which the carbon occupation is random) remains antiferromagnetic as in Gd_5Ge_3 with a slight enhancement of T_N to 83 K (Fig. 14). Incidentally, the paramagnetic Curie temperaure θ_p of $Gd_5Ge_3C_{0.33}$ is positive but the compound does not order ferromagnetically. Similar instances have also been recorded earlier in R_5Ge_4 [26] and Gd_5T_3 (T = Si, Ge and Sn) [27], Dy_5Si_3 [20], Tb_5Sn_3 [28] and R_5Sb_3 [29], to quote a few examples. They have been attributed to the presence of both ferro and antiferromagnetic interactions in these compounds. A metamagnetic transition is observed in the isothermal magnetization at 1.6 and

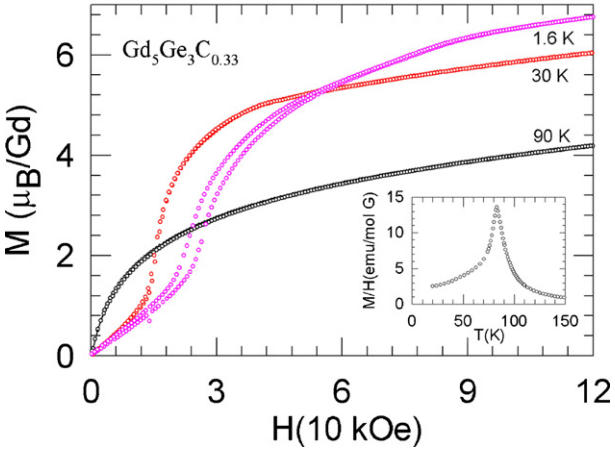

Fig. 14. The field dependence of magnetization of $Gd_5Ge_3C_{0.33}$ up to 120 kOe at 1.6, 30 and 90 K. The inset shows the low field ($H = 50$ Oe) magnetization M/H below 150 K.

30 K at 24 and 13 kOe, respectively. The magnetization plot at 1.6 K shows irreversibility in a certain range of field values and attains a value of 6.8 μ_B/Gd ion at 120 kOe, close to the free ion value of 7 μ_B.

3.3. Electrical resistivity and heat capacity

Since the magnetic behavior of some cerium compounds arises due to an interplay of competing RKKY indirect exchange interaction and the single-ion Kondo interaction, the magnetic properties of $Ce_{15}Ge_9C$ were further explored by measuring its electrical resistivity (1.6–300 K) and low temperature heat capacity (1.8–50 K), together with those of the non-magnetic reference analog $La_{15}Ge_9C$. The electrical resistivity of reference $La_{15}Ge_9C$ (inset of Fig. 15) decreases as the sample is cooled to low temperatures and thus shows expected metallic behavior arising due to the scattering of the charge carriers from phonons. The resistivity of $Ce_{15}Ge_9C$ decreases with temperature as the sample is cooled below 300 K, goes through a broad minimum at ~25 K, and exhibits a sharp peak at 10 K. It decreases with temperature below 10 K, before exhibiting another upturn at ~4 K. The 4*f* contribution to the resistivity, ρ_{4f}, is usually obtained by subtracting the resistivity of non-magnetic La analog from the isotypic magnetic compound. But in the present case the resistivity of $La_{15}Ge_9C$ is higher than that of the Ce compound and ρ_{4f} cannot be estimated. The presence of micro cracks in the La compound could be a possible reason for its higher resistivity. The upturn in the resistivity below 25 K

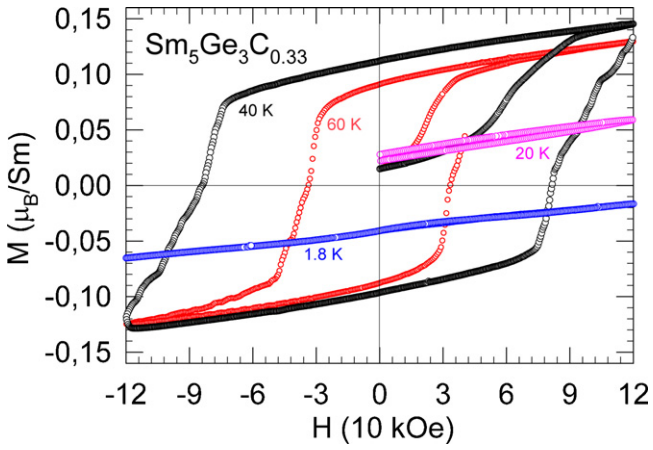

Fig. 13. The hysteresis loops of $Sm_5Ge_3C_{0.33}$ at 1.8, 20, 40 and 60 K up to 120 kOe.

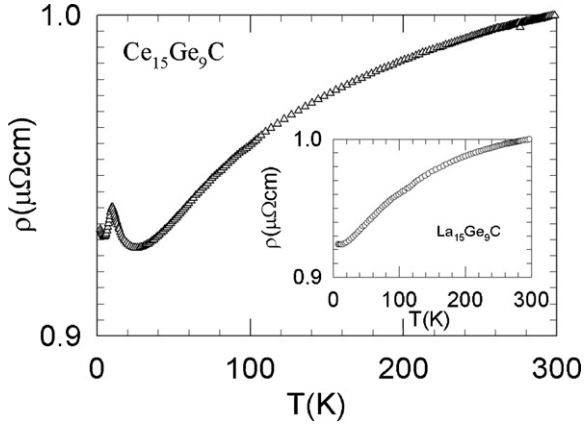

Fig. 15. The electrical resistivity of $Ce_{15}Ge_9C$ (main panel) and non-magnetic, reference compound $La_{15}Ge_9C$ (inset) between 1.7 and 300 K.

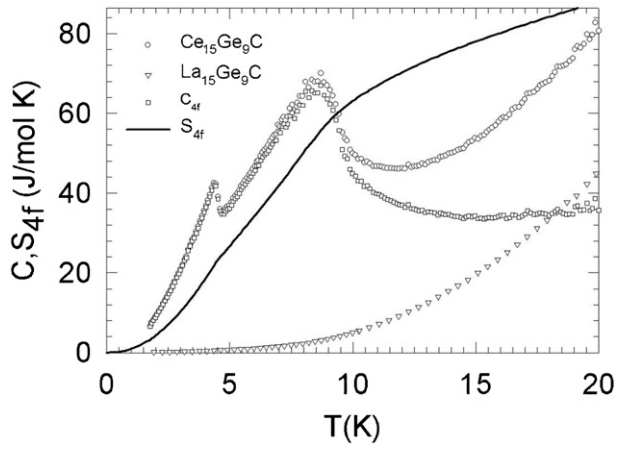

Fig. 16. The heat capacity of $Ce_{15}Ge_9C$ and the non-magnetic, reference compound $La_{15}Ge_9C$ between 1.7 and 20 K. The 4*f* contribution, C_{4f}, and the corresponding entropy, S_{4f}, are also plotted.

in $Ce_{15}Ge_9C$ can in principle be attributed to arise from the Kondo scattering of the charge carriers and it is in conformity with the large, negative θ_p inferred from the susceptibility data. The peak at 10 K correlates with the magnetic transition at ~8.5 K, as inferred from the magnetization data. At lower temperatures the resistivity decreases due to the gradual freezing of the spin-disorder resistivity. The upturn at ~4 K may have its origin in the re-alignment of the magnetic moments suggested by the ZFC magnetization data (Fig. 8).

The heat capacity of $Ce_{15}Ge_9C$ and $La_{15}Ge_9C$ is plotted in Fig. 16. A fit of the expression $C/T = \gamma + \beta T^2$ to the heat capacity data in $La_{15}Ge_9C$ below 10 K gives $\gamma = 54$ mJ/mol K^2 (= 3.6 mJ/La-mol K^2) which is typical of non-magnetic, paramagnetic La compounds. The 4*f* contribution to the heat capacity, C_{4f}, obtained by subtracting the heat capacity of $La_{15}Ge_9C$ from that of $Ce_{15}Ge_9C$, and the entropy S_{4f} are also plotted. The heat capacity of $Ce_{15}Ge_9C$ shows two peaks at ~8 and ~4.2 K corresponding to two magnetic transitions, which is in overall agreement with the features seen in the magnetization and resistivity data. In the paramagnetic regime C_{4f} initially decreases from the peak at ~8 K down to ~15 K and then increases up to the highest measured temperature of 45 K (the data are shown up to 20 K only). A substantial short-range order above T_C and/or a Schottky contribution arising from closely lying excited crystal electric field levels can be invoked to explain the persistence of a finite C_{4f} to such high temperatures and the increase of C_{4f} above 16 K. The entropy S_{4f}/Ce-mol attains a value of 4.2 J/Ce-mol K at 10 K which is less than $R\ln 2$ (5.76 J/Ce-mol K) arising from the crystal electric field doublet ground state with effective spin $s = ½$. It attains the theoretical value at 18 K much above the magnetic transition. Since most likely there is Schottky contribution to the heat capacity at low temperatures, S_{4f} due to the magnetic order alone would be even lower, implying indirectly the non-magnetic nature of some Ce ions located at the four in-equivalent symmetry sites of the unit cell. Thus both resistivity and the heat capacity data indicate the existence of Kondo interaction in $Ce_{15}Ge_9C$.

3.4. Overall remarks

With the exception of $Gd_5Ge_3C_{0.33}$, the addition of carbon leads mostly to a ferromagnetic state in the ternary compounds, though ferrimagnetic ordering is also inferred in some cases. Interestingly, the effect of carbon addition to these compounds is similar to that in Mn_5Si_3 and Mn_5Ge_3. The antiferromagnetic Mn_5Si_3 changes to a ferromagnet in $Mn_5Si_3C_x$ thin films with a T_C of 350 K at $x \sim 0.8$, while the Curie temperature of Mn_5Ge_3 is enhanced from 300 K to a maximum of 442 K in $Mn_5Ge_3C_x$ thin films [30–32]. The enhancement of ferromagnetic stability in Mn_5X_3 compounds due to the addition of carbon has been proposed to an increased interaction between Mn atoms mediated by the interstitially incorporated carbon such that the occupation of the *sp* states overlapping with the *d* bands is changed by Mn–C and X–C interactions leading to a spontaneous magnetization. In the present compounds the electronic shells of the 4*f*-derived magnetic moments are well localized (apart possibly from the Ce analog) and addition of carbon will leave the 4*f* states virtually unaltered unlike the 3d states in Mn compounds. The preponderance of ferromagnetic interaction in the superstructure compounds can tentatively be attributed to a change in the sign of the RKKY sum $\sum F(2k_F R_{nm})$, where $F(x) = (x\cos x - \sin x)/x^4$, k_F is the Fermi wave vector and R_{nm} is the distance between the rare earth ions located at two distinct sites *n* and *m* and the origin is taken as a rare earth site; theoretical calculations would be helpful to corroborate this assumption.

As we have previously mentioned, the solubility of carbon in some of the R_5Si_3 compounds has been investigated in the literature; Er_5Si_3, for example, forms as single phase for compositions up to $Er_5Si_3C_x$ ($x = 2$) [33]. Regions of superstructure formation separated by disordered structures were observed as a function of *x*. Similarly, La_5Ge_3C is also known to exist [2]. It would be therefore interesting to check whether the concentration of interstitial carbon in R_5Ge_3 compounds can be increased further and to investigate the changes brought about in the lattice symmetry and magnetic behavior of $R_5X_3C_y$ (X = Si and Ge; $y > 0.33$). We plan to carry out such studies in future.

Appendix A. Supplementary data

Supplementary data associated with this article can be found, in the online version, at doi:10.1016/j.jallcom.2011.03.092.

References

[1] P. Villars, L.D. Calvert, Pearson's Handbook of Crystallographic Data for Intermetallic Phases, second ed., American Society for Metals, Metals Park, OH, 1991.
[2] I. Mayer, I. Shidlovsky, Inorg. Chem. 8 (1969) 1240–1243.
[3] I. Mayer, I. Felner, J. Less-Common Met. 37 (1974) 171–173.
[4] G.Y.M. Al-Shahery, R. Steadman, I.J. McColm, J. Less-Common Met. 92 (1983) 329–338.
[5] A.M. Guloy, J.D. Corbett, Inorg. Chem. 35 (1996) 4669–4675.
[6] Shah, et al., Proceedings of the DAE Solid State Physics Symposium, Mysore (IN), 2007;
Wrubl, et al., XXXVII Congresso Nazionale di Chimica Fisica, Genova (IT), 2008.
[7] J. Rodriguez-Carvajal, Phys. B 192 (1993) 55–69.
[8] G.M. Sheldrick, SHELXS-97 Program for Crystal Structure Solution, University of Göttingen, 1997.
[9] G.M. Sheldrick, SHELXL-97, Program for Refinement of Crystal Structures, University of Göttingen, 1997.
[10] L.W. Finger, M. Kroekerb, B.H. Toby, J. Appl. Crystallogr. 40 (2007) 188–192.
[11] K. Yvon, W. Jeitschko, E. Parthé, J. Appl. Crystallogr. 10 (1977) 73–74.
[12] E. Teatum, K.A. Gschneidner (Eds.), The Crystal Chemistry and Physics of Metals and Alloys, W. Pearson ed., Wiley, 1972, p. 151.
[13] J. Shi, H. Izumi, K. Machida, G. Adachi, J. Alloys Compd. 240 (1996) 156–163.
[14] K.H.J. Buschow, J.F. Fast, Phys. Status Sol 21 (1967) 593–600.
[15] S.K. Dhar, P. Manfrinetti, A. Palenzona, M. Pani, J. Alloys Compd. 347 (2002) 1–8.
[16] P. Schobinger-Papamantellos, K.H.J. Buschow, J. Magn. Magn. Mater. 49 (1985) 349–356.
[17] M. Kurisu, T. Mitsumata, I. Oguro, Phys. B 259–261 (1999) 96–98.
[18] T. Tsutaoka, Y. Nishiume, T. Tokunaga, J. Magn. Magn. Mater. 272–276 (2004) E421–E422.
[19] I.P. Semitelou, H. Konguetsof, J.K. Yakinthos, E. Roudaut, J. Magn. Magn. Mater. 79 (1989) 131–135.
[20] I.P. Semitelou, J.K. Yakinthos, J. Magn. Magn. Mater. 265 (2003) 152–155.
[21] I.P. Semitelou, J.K. Yakinthos, E. Roudaut, J. Phys. Chem. Solids 56 (1995) 891–894.
[22] P. Schobinger-Papamantellos, J. Magn. Magn. Mater. 28 (1982) 97–108.
[23] A. Morozkin, O. Isnard, P. Henry, P. Manfrinetti, J. Alloys Compd. 464 (2008) 219–226.
[24] A. Morozkin, O. Isnard, P. Henry, P. Manfrinetti, J. Magn. Magn. Mater. 307 (2006) 124–127.
[25] D.A. Joshi, A. Thamizhavel, S.K. Dhar, Phys. Rev. B 79 (2009) 014425.

[26] F. Holtzberg, R.J. Gambino, T.R. McGuire, J. Phys. Chem. Solids 28 (1967) 2283–2289.
[27] F. Canepa, S. Cirafici, M. Napoletano, J. Alloys Compd. 335 (2002) L1–L4.
[28] A. Tanaka, T. Tsutaoka, T. Tokunaga, J. Alloys Compd. 408–412 (2006) 184–186.
[29] J.K. Yakinthos, I.P. Semitelou, J. Magn. Magn. Mater. 36 (1983) 136–140.
[30] M. Gajdzik, C. Sürgers, M.T. Kelemen, H.v. Löhneysen, J. Magn. Magn. Mater. 221 (2000) 248–254.
[31] C. Sürgers, K. Potzger, T. Strache, W. Möller, G. Fischer, N. Joshi, H.v. Löhneysen, Appl. Phys. Lett. 93 (2008) 062503.
[32] B. Gopalakrishnan, C. Sürgers, R. Montbrun, A. Singh, M. Uhlarz, H.v. Löhneysen, Phys. Rev. B 77 (2008) 104414.
[33] G.Y.M. Al-Shahery, D.W. Jones, I.J. McColm, R. Steadman, J. Less-Common Met. 85 (1982) 233–245.